Journal of Physics Communications

PAPER • **OPEN ACCESS**

Analytic treatment of the thermoelectric properties for two coupled quantum dots threaded by magnetic fields

To cite this article: G Menichetti *et al* 2018 *J. Phys. Commun.* **2** 055026

View the article online for updates and enhancements.

Related content

- Seebeck effect in molecular junctions
Natalya A Zimbovskaya
- Thermoelectric energy harvesting with quantum dots
Björn Sothmann, Rafael Sánchez and Andrew N Jordan
- The role of Coulomb interaction in thermoelectric effects of an Aharonov–Bohminterferometer
Yu-Shen Liu, De-Bao Zhang, Xi-Feng Yang et al.

This content was downloaded from IP address 93.148.21.75 on 24/05/2018 at 19:08

Journal of Physics Communications

CrossMark

OPEN ACCESS

RECEIVED
30 March 2018

REVISED
7 May 2018

ACCEPTED FOR PUBLICATION
11 May 2018

PUBLISHED
23 May 2018

Original content from this work may be used under the terms of the Creative Commons Attribution 3.0 licence.

Any further distribution of this work must maintain attribution to the author(s) and the title of the work, journal citation and DOI.

PAPER

Analytic treatment of the thermoelectric properties for two coupled quantum dots threaded by magnetic fields

G Menichetti[1], **G Grosso**[2,3] **and G Pastori Parravicini**[2,4]

[1] Istituto Italiano di Tecnologia, Graphene Labs, Via Morego, 30, I-16163 Genova, Italy
[2] Dipartimento di Fisica 'E. Fermi', Università di Pisa, Largo Pontecorvo 3, I-56127 Pisa, Italy
[3] NEST, Istituto Nanoscienze-CNR, Piazza San Silvestro 12, I-56127 Pisa, Italy
[4] Dipartimento di Fisica 'A. Volta', Università di Pavia, Via A. Bassi, I-27100 Pisa, Italy

E-mail: guido.menichetti@itt.it

Keywords: quantum transport, thermoelectric effects, double quantum dots, green's function methods, quantum interference effects

Supplementary material for this article is available online

Abstract

Coupled double quantum dots (c-2QD) connected to leads have been widely adopted as prototype model systems to verify interference effects on quantum transport at the nanoscale. We provide here an analytic study of the thermoelectric properties of c-2QD systems pierced by a uniform magnetic field. Fully analytic and easy-to-use expressions are derived for all the kinetic functionals of interest. Within the Green's function formalism, our results allow a simple inexpensive procedure for the theoretical description of the thermoelectric phenomena for different chemical potentials and temperatures of the reservoirs, different threading magnetic fluxes, dot energies and interdot interactions; moreover they provide an intuitive guide to parametrize the system Hamiltonian for the design of best performing realistic devices. We have found that the thermopower S can be enhanced by more than ten times and the figure of merit ZT by more than hundred times by the presence of a threading magnetic field. Most important, we show that the magnetic flux increases also the performance of the device under maximum power output conditions.

1. Introduction

Quantum dot systems have attracted enormous interest as workable thermoelectric device candidates for the study of electronic and thermal quantum transport at the nanoscale. The origin of such an interest both from the theoretical and the experimental side, resides in the potential they offer, as artificial nanoscale junctions, to explore a large variety of thermoelectric effects. Relevance of nanostructures as performing energy harvesting devices was envisaged in the pioneering paper of Hick and Dresselhaus [1]. Since then nanoscale thermoelectricity has been addressed by an increasing number of theoretical and experimental works; a perspective of the field can be found in the focus point collection in [2] and in the articles appeared in [3]. In particular, interference Ahronov-Bohm [4–7], Fano [8–11], Dicke [12, 13] and Mach-Zehnder [14, 15] effects, inter- and intra-dot correlation effects [16–18], coherent transport modification by external magnetic fields and gate voltages. [19–21], have been exploited to control the performance of thermoelectric heat devices.

The system composed by two single-level quantum dots coupled to each other (c-2QD) via metallic leads, in two terminal or multiterminal setups [22], and via an interdot tunneling are most appropriate to probe how the Hamiltonian system parameters and external conditions can be varied to optimize the energy conversion efficiency and the output power of the thermoelectric device. This is a demanding task because such parameters often play conflicting roles in the optimization process. Strategies for increasing thermoelectric performances utilizing a steep slope in the transmission function $\mathcal{T}$ (E), or its specific shape, or its resonances, have been well described in [23] where also a comparison between the thermoelectric efficiency of inorganic and organic materials is discussed.

© 2018 The Author(s). Published by IOP Publishing Ltd

It is worth noticing that in addition to the numerous papers dealing with two quantum dots tunnel-coupled to the leads and between themselves, also Coulomb-coupled quantum dots [24, 25] have attracted increasing interest in the recent years [for a general perspective see [26]. This has been motivated by the advances in the fabrication of nano-devices, energy harvesting [22] with quantum dots, and the experimental possibility to taylor TE properties exploiting Coulomb interaction and the charge carriers correlation [27]. Moreover, in recent years parallel coupled quantum dots made of semiconductors with high spin-orbit interaction have proven promising systems to realize two-spin qubit in quantum information processing [28, 29].

Enhancing thermoelectric performance in linear regimes, requires maximization of the dimensionless thermoelectric figure of merit $ZT = \sigma S^2 T/\kappa$ where σ is the electrical conductance, S the thermopower (Seebeck) coefficient, T is the temperature and $\kappa = \kappa_e + \kappa_p$ is the thermal conductance (which includes electronic and lattice contributions). In the search of optimal thermoelectric response of the device, most important quantities are its maximum efficiency as thermoelectric generator, and the efficiency at the maximum of the output power.

A crucial aspect both in the implementation of experimental methods [30], and in the evaluation of the thermoelectric response of bulk and nanostructured materials, is the wide parameters range to be explored simultaneously to determine its optimal functioning. In this context, the possibility of using analytic expressions for all the involved thermoelectric functions greatly simplifies the task. In the literature, the analytic treatment of the c-2QD is confined at sufficiently small temperatures by means of the Sommerfeld expansion, extended when necessary to fourth order in k_BT in the evaluation of kinetic parameters [9]. In the case of Lorentzian shape of the transmission function, analytic expressions of the thermoelectric transport coefficients have been obtained in terms of digamma functions [31]. In the more complicated transmission function of coupled double dot, we provide here, in terms of trigamma functions [32, 33], analytic expressions for the relevant quantities describing the thermoelectric behavior of a c-2QD. The description of the c-2QD electronic transport is performed within the Green's function framework. We have exploited such expressions to study the variation of Seebeck coefficient, figure of merit, energy conversion efficiency and output power, as function of temperatures and chemical potentials of the reservoirs, and of the magnetic field threading the c-2QD. In particular we focus on the thermoelectric efficiency of the c-2QD device, in contact with left and right reservoirs, when it operates at maximum output power conditions.

We adopt the convention that the left reservoir is the hotter one ($T_L > T_R$) while no *a priori* assumption is done on the relative position of the chemical potentials μ_L and μ_R of the left and right reservoirs. We consider a two-terminal quantum dot setup, stationary transport conditions, absence of lattice contributions to thermal conductivity ($k \approx k_e$), and no electronic correlation effects. The general expression for thermoelectric transport charge current I through the c-2QD, in stationary conditions, is given by [34]

$$I = \frac{-e}{h}\int_{-\infty}^{+\infty} dE\ \mathcal{T}(E)[f_L(E) - f_R(E)] \tag{1}$$

where $f_{L,R}$ denote the Fermi functions of the two reservoirs. The electric power output ($\mathcal{P}$(E) > 0) is given by

$$\mathcal{P} = -I\Delta V = \frac{1}{h}(\mu_R - \mu_L)\int dE\ \mathcal{T}(E)[f_L(E) - f_R(E)]. \tag{2}$$

where $\Delta V = (\mu_L - \mu_R)/(-e)$ is the voltage drop and $e = |e|$ is absolute value of the electron charge.

The thermoelectric efficiency of the device is given by the ratio between the work done and the heat extracted from the high temperature reservoir:

$$\eta = \frac{W}{Q_L} = \frac{(Q_L - Q_R)}{Q_L}. \tag{3}$$

In steady state conditions the heats per unit time are the thermal currents and W per unit time is the output power $\mathcal{P}$. Then

$$\eta = (\mu_R - \mu_L)\frac{\int dE\ \mathcal{T}(E)[f_L(E) - f_R(E)]}{\int dE(E - \mu_L)\ \mathcal{T}(E)[f_L(E) - f_R(E)]}. \tag{4}$$

Expressions from (1) to (4) depend on the thermodynamic parameters μ_L, T_L, μ_R, T_R and on the c-2QD transmission function $\mathcal{T}$(E), and hold in the linear and nonlinear regimes. In this paper we are interested in the linear response of the system so that $\Delta\mu = \mu_L - \mu_R$ and $\Delta T = T_L - T_R$ are infinitesimal quantities. To first order in ΔT and $\Delta\mu$, we can thus write

$$f_L(E) - f_R(E) = \left(-\frac{\partial f_L}{\partial E}\right)\left[\Delta\mu + (E - \mu_L)\frac{\Delta T}{T_L}\right].$$

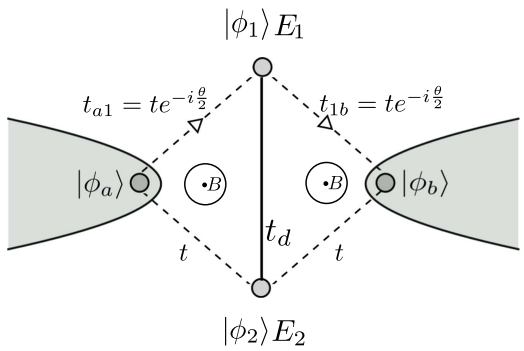

Figure 1. Schematic representation of the double dot electronic system in a symmetric environment for the analysis of thermoelectric properties. In the absence of magnetic field, the four hopping parameters of the ring are equal to t (taken as real). The magnetic field, in the chosen gauge, modifies $t_{a1} \to te^{-i\theta/2} = t_{1a}^*$ and $t_{1b} \to te^{-i\theta/2} = t_{b1}^*$, where $\theta = 2\pi\Phi(B)/\Phi_0$, $\Phi(B)$ is the flux of the magnetic field through the entire two-loop (ϕ_a, ϕ_1 , ϕ_b, ϕ_2) plaquette, and $\Phi_0 = hc/e$ is the quantum of flux. In the case of degeneracy $E_1 = E_2 = E_d$.

For convenience, the thermodynamic parameters μ_L, T_L and the Fermi function f_L are denoted below dropping the now inessential subscript L.

In section 2 we report details on the c-2QD system and its description in terms of localized functions. In section 3 we provide analytic expressions of the transport parameters relevant to control and design of the thermoelectric response of the c-2QD, in the linear response regime. Application of the above expressions and discussion of the results are reported in section 4 where contour plots are reported to better evidence the energy and magnetic field values eventually responsible of efficiency at the maximum output power. We have found that the thermopower S may be enhanced by more than ten times and the figure of merit ZT by more than hundred times due to a threading magnetic field. We look for chemical potential and magnetic flux values which give the maximum output power and demonstrate that the magnetic flux also increases the corresponding efficiency. Section 5 contains our conclusions. Several useful mathematical details are contained in the Supplementary Material sections.

2. System description and model

In this section we establish a localized basis model for the c-2QD electronic system in contact with the left and right reservoirs, in the presence of a threading magnetic field.

Consider a double dot electronic system, with a single orbital per dot, described within the one-electron approximation in the tight-binding framework. The one-electron Hamiltonian can be partitioned in the left lead, central device, right lead, and coupling interaction

$$H = H^{(left)} + H^{(dots)} + H^{(right)} + W^{(dots-leads)}. \tag{5}$$

The electronic system is schematically pictured in figure 1, where the presence of a uniform magnetic field is also considered.

The central device, a double dot molecule, is described by the Hamiltonian of the type in the bra-ket notations

$$H^{(dots)} = E_d|\phi_1\rangle\langle\phi_1| + E_d|\phi_2\rangle\langle\phi_2| + t_d|\phi_1\rangle\langle\phi_2| + t_d|\phi_2\rangle\langle\phi_1|, \tag{6}$$

where E_d is the energy of both dots orbitals ϕ_1, ϕ_2, and t_d (supposed real and negative) is the off-diagonal coupling between the two dots.

For what concerns the description of two electrodes not yet coupled to the dots, we can proceed as follows. Consider, for instance, the left lead and specifically the 'left seed state' $|\phi_a>$ that carries the coupling with the central device. The effect of all the other (infinite) degrees of freedom of the left electrode are embodied in the Green's function g_{aa} on the end seed state. In principle, the Lanczos procedure can be applied to generate the Lanczos chain and, then, to determine the Green's function [see for instance [35]]. The same considerations apply for the right lead. We have

$$g_{aa}^R(E) = \langle\phi_a|\frac{1}{E - H^{(left)} + i\eta}|\phi_a\rangle; \quad g_{bb}^R(E) = \langle\phi_b|\frac{1}{E - H^{(right)} + i\eta}|\phi_b\rangle. \tag{7}$$

Following the routinely adopted 'wide-band approximation' we consider explicitly only the imaginary part of the above Green's functions and disregard the energy dependence. The leads are replaced by the corresponding end states, with the retarded and advanced Green's functions purely imaginary quantities, independent from

energy. In a symmetric geometrical environment, we have

$$g^R_{aa}(E) = g^R_{bb}(E) \approx -i\pi\rho, \quad g^A_{aa}(E) = g^A_{bb}(E) \approx +i\pi\rho \qquad (\rho > 0), \tag{8}$$

where $\rho = -(1/\pi)\,\mathrm{Im}\, g^R$ represents the local density-of-states, assumed to be constant in the typical energy region of actual interest.

The coupling between leads and central device in the absence of magnetic field is represented by a loop with nearest neighbor interaction t (taken as real for simplicity). In the presence of magnetic field, appropriate Peierls phases are introduced. The Berry phases corresponding to the magnetic field are set on the hopping parameters connecting the upper quantum dot ϕ_1 with the end orbitals ϕ_a, ϕ_b of the electrodes:

$$\begin{aligned} W^{(dots-leads)} = {} & te^{-i\theta/2)}|\phi_a\rangle\langle\phi_1| + te^{i\theta/2)}|\phi_1\rangle\langle\phi_a| + t|\phi_a\rangle\langle\phi_2| + t|\phi_2\rangle\langle\phi_a| \\ & + te^{i\theta/2)}|\phi_b\rangle\langle\phi_1| + te^{-i\theta/2)}|\phi_1\rangle\langle\phi_b| + t|\phi_b\rangle\langle\phi_2| + t|\phi_2\rangle\langle\phi_b|. \end{aligned} \tag{9}$$

We have now all the ingredients for the calculation of the Green's function and of the transmission function of the electronic device.

2.1. Green's function of the degenerate double dot in magnetic fields

The central part of the device is constituted by the two orbitals of the two quantum dots, coupled one to the other. We can use the renormalization-decimation procedure to fully eliminate the degrees of freedom of the leads, now represented by the end seed states $|\phi_a>$ and $|\phi_b>$ [see for instance [35]]. The retarded self-energies produced by the left lead on the central device become

$$\begin{aligned} \Sigma^{R(left)}_{11} &= t_{1a} g^R_{aa} t_{a1} = -i\pi\rho\, t^2 \\ \Sigma^{R(left)}_{12} &= t_{1a} g^R_{aa} t_{a2} = -i\pi\rho\, t^2 e^{i\theta/2} \\ \Sigma^{R(left)}_{21} &= t_{2a} g^R_{aa} t_{a1} = -i\pi\rho\, t^2 e^{-i\theta/2} \\ \Sigma^{R(left)}_{22} &= t_{2a} g^R_{aa} t_{a2} = -i\pi\rho\, t^2. \end{aligned} \tag{10}$$

Similar procedures can be followed for the right lead and for the advanced self-energies.

It is convenient to define the real and positive quantity $\gamma/2 = \pi\rho\, t^2 > 0$. The total self-energies of the left and right leads are then

$$\Sigma^R = \Sigma^{R(left)} + \Sigma^{R(right)} = -i\gamma \begin{bmatrix} 1 & \cos(\theta/2) \\ \cos(\theta/2) & 1 \end{bmatrix}, \quad \Sigma^A = i\gamma \begin{bmatrix} 1 & \cos(\theta/2) \\ \cos(\theta/2) & 1 \end{bmatrix}. \tag{11a}$$

Finally the coupling parameters are given by the expressions

$$\Gamma^{(left)} = i[\Sigma^{R(left)} - \Sigma^{A(left)}] = \gamma \begin{bmatrix} 1 & e^{i\theta/2} \\ e^{-i\theta/2} & 1 \end{bmatrix}, \quad \Gamma^{(right)} = \gamma \begin{bmatrix} 1 & e^{-i\theta/2} \\ e^{i\theta/2} & 1 \end{bmatrix}. \tag{11b}$$

It should be noticed that the self-energies Σ and the broadening parameters Γ depend on the applied magnetic field, but are completely independent from the energy variable. This nice feature is a consequence of the wide band approximation and fosters the possibility of a fully analytic treatment of transport parameters, which is a key aspect of this article.

The retarded effective Hamiltonian for the double-dot in the central device, after the full decimation procedure of the leads, is given by the expression

$$H^{R(eff)} = H^{(dots)} + \Sigma^R = \begin{bmatrix} E_d & t_d \\ t_d & E_d \end{bmatrix} - i\gamma \begin{bmatrix} 1 & \cos(\theta/2) \\ \cos(\theta/2) & 1 \end{bmatrix}.$$

The retarded Green's function is represented by the symmetric matrix

$$G^R(E) = \frac{1}{E - H^{R(eff)}} = \frac{1}{D^R(E)} \begin{bmatrix} E - E_d + i\gamma & t_d - i\gamma\cos(\theta/2) \\ t_d - i\gamma\cos(\theta/2) & E - E_d + i\gamma \end{bmatrix}, \tag{12a}$$

where

$$D^R(E) = (E - E_d + i\gamma)^2 - [\, t_d - i\gamma\cos(\theta/2)\,]^2\,. \tag{12b}$$

The advanced Green's function is the hermitian conjugate of the retarded one. Since the matrix $G^R(E)$ in equation (12) is symmetric, it follows

$$G^A(E) = [G^R(E)]^*. \tag{13}$$

2.2. Transmission function of the symmetric double dot in magnetic fields

We can now proceed to the explicit calculation of the transmission function $\mathcal{T}(E)$ of the double dots, coupled one to the other and immersed in magnetic fields. Using the general Keldysh nonequilibrium formalism (applicable to interacting or noninteracting systems) or the Landauer-Büttiker procedure (specific for the latter case) [see for instance [36, 37]], we have that the transmission coefficient of the non-interacting nanostructure is given by the familiar relation

$$\mathcal{T}(E) = \mathrm{Tr}\,[\Gamma^{(left)} G^R(E) \Gamma^{(right)} G^A(E)], \tag{14}$$

where we have taken notice that, in the wide band approximation, the left and right coupling are independent from energy.

To perform the product of the four matrices in equation (14), we begin to consider the product of the first two matrices. Using equation (11*b*) and equation (12) one obtains

$$\begin{aligned}\Gamma^{(left)} G^R(E) &= \frac{\gamma}{D^R(E)} \begin{bmatrix} 1 & e^{i\theta/2} \\ e^{-i\theta/2} & 1 \end{bmatrix} \begin{bmatrix} E - E_d + i\gamma & t_d - i\frac{\gamma}{2}(e^{i\theta/2} + e^{-i\theta/2}) \\ t_d - i\frac{\gamma}{2}(e^{i\theta/2} + e^{-i\theta/2}) & E - E_d + i\gamma \end{bmatrix} \\ &= \frac{\gamma}{D^R(E)} \begin{bmatrix} E - E_d - i\frac{\gamma}{2}(e^{i\theta} - 1) + t_d e^{i\theta/2} & e^{i\theta/2}(E - E_d) - i\frac{\gamma}{2}(-e^{i\theta/2} + e^{-i\theta/2}) + t_d \\ e^{-i\theta/2}(E - E_d) - i\frac{\gamma}{2}(e^{i\theta/2} - e^{-i\theta/2}) + t_d & E - E_d - i\frac{\gamma}{2}(-1 + e^{-i\theta}) + t_d e^{-i\theta/2} \end{bmatrix}. \end{aligned} \tag{15}$$

From equation (11*b*) and equation (13), we also have

$$\Gamma^{(right)} G^A(E) = [\Gamma^{(left)} G^R(E)]^*.$$

Multiplication of the matrix of equation (15) by its complex conjugate matrix, followed by the trace operation, gives the transmission function.

After somewhat lengthy but straight manipulations one obtains the expression of the transmission function of a coupled double quantum dot in a uniform magnetic field and symmetrical geometry:

$$\mathcal{T}(E) = \frac{4\gamma^2}{D^R(E) D^A(E)} [\cos(\theta/2) \cdot (E - E_d) + t_d\ ]^2 \tag{16a}$$

where

$$D^R(E) = [E - E_d - t_d + 2i\gamma \cos^2(\theta/4)][E - E_d + t_d + 2i\gamma \sin^2(\theta/4)]. \tag{16b}$$

The same procedure can be exploited in the case the dot levels are non degenerate, or the geometric environment is non-symmetric, the magnetic field is nonuniform, for multilevel dots, and other similar situations.

For instance, in the case of a non-degenerate double quantum dot, with energy levels $E_1 \neq E_2$ in a symmetric geometrical environment the transmission function becomes

$$\begin{aligned}\mathcal{T}(E) = \frac{\gamma^2}{D^R(E) D^A(E)} &[(E - E_1)^2 + (E - E_2)^2 + 2\cos\theta \cdot (E - E_1)(E - E_2) \\ &+ 4t_d \cos(\theta/2) \cdot (2E - E_1 - E_2) + 4t_d^2\ ],\end{aligned} \tag{17a}$$

where

$$D^R(E) = (E - E_1 + i\gamma)(E - E_2 + i\gamma) - [\ t_d - i\gamma \cos(\theta/2)\ ]^2 \equiv [D^A(E)]^*. \tag{17b}$$

In the case of degeneracy $E_1 = E_2 = E_d$, one recovers back equation (16).

2.3. Magnetic field effects on the transmission function

The transmission function, given in equation (16), versus θ is periodic with period 4π, corresponding to two additional flux quanta, or equivalently to one flux quantum for each of the two loops of figure 1.

In the absence of magnetic fields (or in the presence of an even number of flux quanta), from equations (16) one obtains

$$\mathcal{T}(E, 0) = \frac{4\gamma^2}{(E - E_d - t_d)^2 + 4\gamma^2}, \tag{18}$$

which is just a Lorentzian function centered at $E = E_d + t_d = E_d - |t_d|$, the *bonding* state, and effective width $\Gamma_{eff} = 2\gamma$. In the presence of one flux quantum (or any odd integer number of flux quanta) equation (16) gives

$$\mathcal{T}(E, 2\pi) = \frac{4\gamma^2}{(E - E_d + t_d)^2 + 4\gamma^2}, \tag{19}$$

which is a Lorentzian function centered at $E = E_d - t_d = E_d + |t_d|$, the *anti-bonding* state, and effective width $\Gamma_{eff} = 2\gamma$. At semi-integer flux quanta $\theta = \pi$ (or any odd integer number of π) the transmission function versus

E takes the symmetric structure with respect to the dot energy E_d, with expression

$$\mathcal{T}(E,\,\pi) = \frac{4\gamma^2 t_d^2}{[(E - E_d - t_d)^2 + \gamma^2][(E - E_d + t_d)^2 + \gamma^2]}. \tag{20}$$

For $\gamma \ll |t_d|$ (including also $\gamma \leqslant |t_d|$) the transmission function of equation (20) exhibits two peaks at $\pm(t_d^2 - \gamma^2)^{1/2}$, and a valley around $E = 0$. The two peaks are well separated if $|t_d| \gg \gamma$.

It is of much importance to notice that, apart the special values $\theta = 0, \pi, 2\pi, 3\pi$ (modulus 4π) discussed above, for finite values of E, the transmission function of equation (16) has a unique zero; namely:

$$\mathcal{T}(E,\,\theta) \equiv 0 \qquad \Longrightarrow \qquad E \equiv E_d - \frac{t_d}{\cos(\theta/2)} = E_d + \frac{|t_d|}{\cos(\theta/2)}. \tag{21}$$

Thus the antiresonance is at the right of the anti-bonding state for $0 < \theta < \pi$, while it is at the left of the bonding state for $\pi < \theta < 2\pi$.

From the above discussion, it is seen how the application of the magnetic field may transform a trivial unstructured Lorentzian function into a peaked-valley-peaked-valley (with zero minimum) sharply structured function, with much benefit in the entailed thermoelectric properties. In general, the transmission function can be qualitatively described as the sum of a Lorentzian-like curve around the bonding level and a Fano-like curve around the anti-bonding level (or vice versa, depending on the applied magnetic field), with separation connected to the coupling energy $|t_d|$.

3. Structure of the transmission function and analytic evaluation of the kinetic parameters

Once the transmission function is known, we can access the kinetic transport coefficients that control, in the linear approximation, the thermoelectric properties of the nanoscale device. The kinetic transport coefficients, of order n, in dimensionless form, are linked to the transmission function $\mathcal{T}(E)$ by the relations:

$$K_n = \int_{-\infty}^{+\infty} dE\; \mathcal{T}(E)\, \frac{(E-\mu)^n}{(k_B T)^n} \left(-\frac{\partial f}{\partial E}\right) \qquad (n = 0,\,1,\,2). \tag{22}$$

where μ is the chemical potential, T the absolute temperature, and $f(E, \mu, T)$ the Fermi function.

In the literature, the evaluation of the kinetic coefficients $K_{0,1,2}$ is in general carried out either with the Sommerfeld expansion [38], possibly extended up to fourth order [9], or by numerical integration. A nice aspect of the Sommerfeld expansion is that the procedure is analytic; however it holds only at sufficiently low temperatures and reasonably smooth transmission function in the energy interval k_BT. The alternative procedure, based on numerical integration, requires particular caution because of the presence of sharp resonances and anti-resonance produced by the interference effects of the magnetic fields. The purpose of this section is to develop a brand new analytic procedure for the evaluation of the kinetic parameters, valid for any temperature range and applicable in any desired domain of the other parameters at play.

The first step to elaborate analytically the kinetic functionals requires the examination of the pole structure of $\mathcal{T}(E)$. The transmission function can in fact be resolved into the sum of just two simple poles, with appropriate weighting factors. This is shown in detail in the S1 section of the Supplementary Material[6].

The result is reported in the upper part of table 1. The evaluation of kinetic parameters is now straightforward and their analytic expression is reported in the lower part of table 1 in terms of the trigamma function $\Psi_t(z) = \sum_{n=0}^{\infty} 1/(z+n)^2$. Trigamma functions and Bernoulli-like numbers are the ingredients for the analytic evaluation of the kinetic functional of interest. Details of their analytic evaluation are reported in the S2 section of the Supplementary Material (see footnote 5).

It becomes now routine to investigate the thermoelectric transport properties. Following closely [39], in table 2 we report for sake of completeness the expressions of the electric and thermal conductances, of the Seebeck coefficient and the other transport parameters of interest, in terms of the kinetic coefficients K_0, K_1, and K_2.

In the next section we evaluate magneto transport properties of specific double dot devices, and discuss the variety and wealth of effects occurring in spite of the reasonable simplicity of the model.

4. Results and discussion

We begin to examine a realistic space domain for the thermoelectric device under attention. For molecular junctions, we can set $\gamma \approx 0.25$ eV and $t_d \approx -1.0$ eV. The fact that $|t_d| \gg \gamma$ (almost an order of magnitude)

[6] see Supplementary Material.

Table 1. Transmission function $\mathcal{T}(E)$ and kinetic integrals $K_{0,1,2}$ in analytic form of the symmetric double quantum dot, with two orbitals of the same diagonal energy E_d, coupled together by the off-diagonal hopping element t_d, in the wide band approximation of parameter γ. The phase θ equals $2\pi\,\Phi(B)/\Phi_0$, where $\Phi(B)$ is the flux of magnetic field through the nanodevice in units of a single quantum flux Φ_0. The trigamma function is denoted with Ψ_t.

Transmission function $\mathcal{T}(E)$ for the coupled degenerate double dot
$\mathcal{T}(E) = 8\gamma^2\,\mathrm{Re}\left\{\frac{1}{A_1}\frac{[\cos(\theta/2)\,(E-E_d)+t_d]^2}{E-z_1} + \frac{1}{A_2}\frac{[\cos(\theta/2)\,(E-E_d)+t_d]^2}{E-z_2}\right\}$
where $\begin{cases} A_1 = -16\,i\gamma\cos^2(\theta/4)\,[-i\gamma\cos(\theta/2)+t_d]\,[-i\gamma+t_d] \\ A_2 = -16\,i\gamma\sin^2(\theta/4)\,[+i\gamma\cos(\theta/2)-t_d]\,[-i\gamma-t_d] \\ z_1 = E_d + t_d - i\gamma - i\gamma\cos(\theta/2) \\ z_2 = E_d - t_d - i\gamma + i\gamma\cos(\theta/2). \end{cases}$
Dimensionless kinetic parameters for the degenerate double dot system in the linear regime:
$K_n = \int dE\;\mathcal{T}(E)\frac{(E-\mu)^n}{(k_BT)^n}\left(-\frac{\partial f}{\partial E}\right)$
$K_0 = 8\gamma^2\,\mathrm{Re}\left\{\sum_{m=1}^{2}\frac{1}{A_m}[\cos^2(\theta/2)\,(\mu+z_m-2E_d)+2\cos(\theta/2)\,t_d + \frac{[\cos(\theta/2)\,(z_m-E_d)+t_d]^2}{k_BT}\,J_0\left(\frac{z_m-\mu}{k_BT}\right)]\right\}$
$K_1 = 8\gamma^2\,\mathrm{Re}\left\{\sum_{m=1}^{2}\frac{1}{A_m}\left[\frac{\pi^2}{3}\cos^2(\theta/2)\,k_BT + \frac{[\cos(\theta/2)\,(z_m-E_d)+t_d]^2}{k_BT}\,J_1\left(\frac{z_m-\mu}{k_BT}\right)\right]\right\}$
$K_2 = 8\gamma^2\,\mathrm{Re}\left\{\sum_{m=1}^{2}\frac{1}{A_m}\left[\frac{\pi^2}{3}\cos^2(\theta/2)\,(\mu+z_m-2E_d)+\frac{2\pi^2}{3}\cos(\theta/2)\,t_d + \frac{[\cos(\theta/2)\,(z_m-E_d)+t_d]^2}{k_BT}\,J_2\left(\frac{z_m-\mu}{k_BT}\right)\right]\right\}$
$J_0(w) = \pm\frac{1}{2\pi i}\Psi_t\left(\frac{1}{2}\pm\frac{iw}{2\pi}\right)\quad \mathrm{Im}\,w \lessgtr 0;\;\; J_1(w) = 1 + wJ_0(w);\;\; J_2(w) = w + w^2J_0(w)$

Table 2. Transport parameters in the linear approximation for thermoelectric materials, with electronic transmission function $\mathcal{T}(E)$. The kinetic parameters $K_{0,1,2}$ are defined in dimensionless form. The electric conductance σ, Seebeck coefficient S, power-output $\mathcal{P}$, electronic thermal conductance κ_e, Lorenz number L, performance parameter p, figure of merit ZT and efficiency η are reported. The quantity η_c denotes the Carnot efficiency $\eta_c = \Delta T/T$, where ΔT is the temperature difference between the hot reservoir and the cold one.

Expressions of the thermoelectric functions in terms of the kinetic parameters		
$\sigma = K_0\,\frac{e^2}{h}$	$S = -\frac{K_1}{K_0}\,\frac{k_B}{e}$	$\kappa_e = T\left(K_2 - \frac{K_1^2}{K_0}\right)\left(\frac{k_B^2}{h}\right)$
$\frac{\mathcal{P}}{\eta_c^2} = \frac{1}{4}\,T^2\,\frac{K_1^2}{K_0}\,\frac{k_B^2}{h}$	$L = \frac{K_0K_2 - K_1^2}{K_0^2}\,\frac{k_B^2}{e^2}$	$p = \frac{K_1^2}{K_0K_2}\quad(0 \leqslant p \leqslant 1)$
$ZT = \frac{K_1^2}{K_0K_2 - K_1^2} = \frac{p}{1-p}$	$\frac{\eta}{\eta_c} = \frac{\sqrt{1+ZT}-1}{\sqrt{1+ZT}+1} = \frac{1-\sqrt{1-p}}{1+\sqrt{1-p}}$	
Expressions of the thermoelectric natural units for nanoscale devices		
$\frac{e^2}{h} = 3.874046\cdot 10^{-5}\,\frac{\mathrm{A}}{\mathrm{V}}$;	$\frac{k_B}{e} = 86.17\,\frac{\mu\mathrm{V}}{\mathrm{K}}$;	$\frac{k_B^2}{e^2} = 74.25\cdot 10^{-10}\,\frac{\mathrm{V}^2}{\mathrm{K}^2}$;
$\frac{k_B^2}{h} = 1.8\cdot 10^6\,\frac{\mathrm{eV}}{\mathrm{sec}}\cdot\frac{1}{\mathrm{K}^2} = 0.288\,\frac{\mathrm{pW}}{\mathrm{K}^2}\quad\Longrightarrow\frac{k_B^2T_0^2}{h} = 1.8\cdot 10^6\,\frac{\mathrm{eV}}{\mathrm{sec}} = 0.288\,\mathrm{pW}\quad(T_0 = 1K)$		

assures that in the transmission function the Lorentz lineshape and the Fano lineshape are in general well resolved, with linewidths $2\gamma\cos^2(\theta/4)$ and $2\gamma\sin^2(\theta/4)$, respectively, as it is seen from equation (16). The values of θ explored to better highlight periodicity as function of θ, are in the whole range $[0, 4\pi]$, and in particular $\theta = 0, \pi/2, \pi, 3\pi/2$ and 2π. The range of θ from one flux to two flux quanta ($2\pi < \theta \leqslant 4\pi$) retraces back the range from one flux to zero, and does not need to be considered explicitly. The room temperature considered entails $k_BT = 0.025$ eV. The dot energy E_d is taken as the reference energy and set equal to zero. In summary,: the figures reported below in this section refer to the set of parameters $E_d = 0$, $\gamma = 0.25$ eV, $t_d = -1.0$ eV, $k_BT = 0.025$ eV and $\theta = 0, \pi/2, \pi, 3\pi/2$ and 2π. When useful, other temperatures, phases or parameter domain have been explored and commented (but in general not explicitly reported). In figure 2 the thermoelectric functions of the c-2QD, for varying chemical potential μ and magnetic flux parameter θ are provided. The left panels show the landscape of electrical conductivity σ, electrical thermal conductivity κ_e, Seebeck coefficient S, and figure of merit ZT. The right panels show sections of the same quantities for -2 eV $< \mu < 2$ eV at $\theta = 0, \pi/2, \pi, 3\pi/2$ and 2π, to better highlight their shape and symmetry. The curves profiles reported in the left panels respect the color sequence shown in the corresponding right panels. From

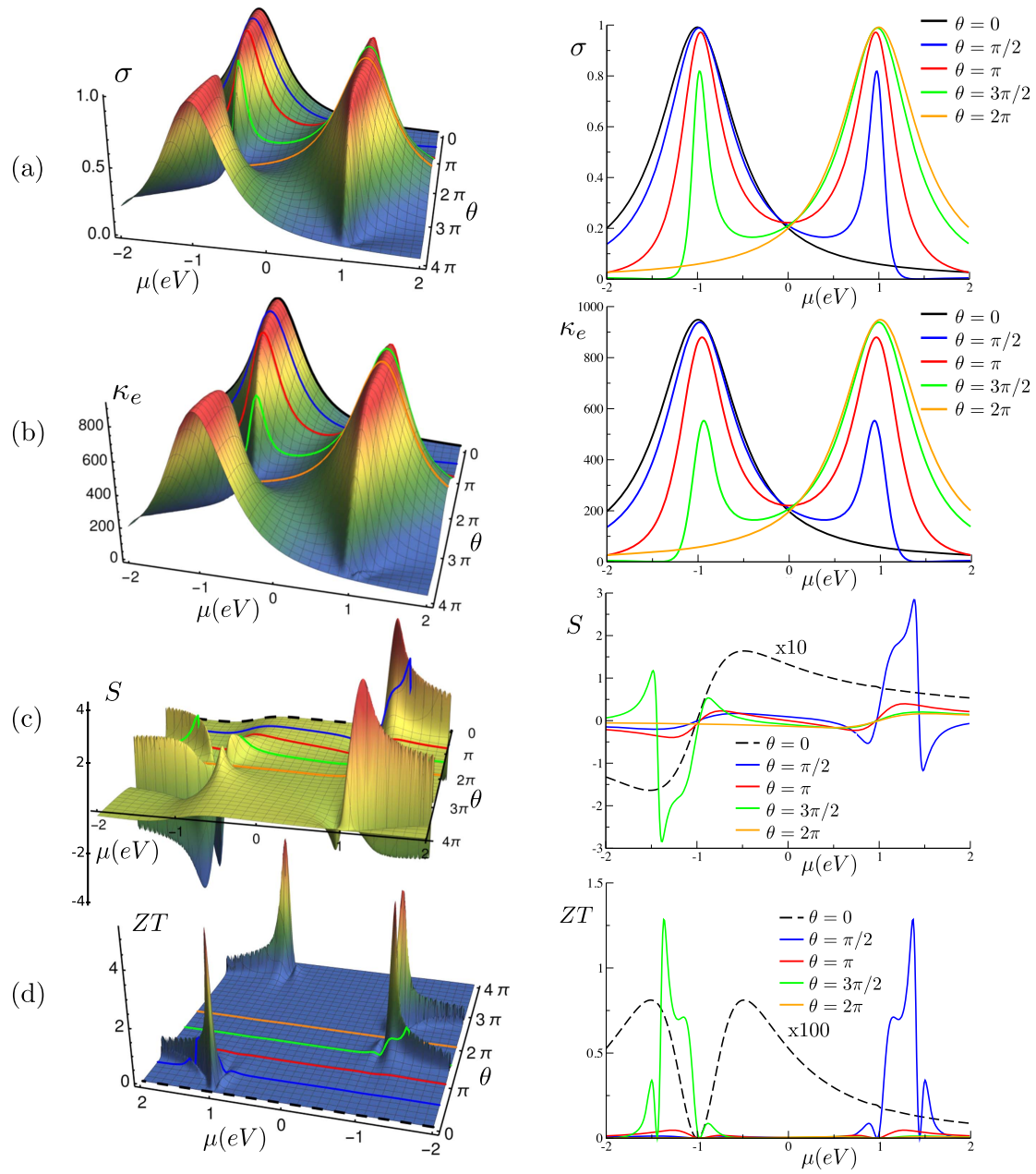

Figure 2. (a) Electrical conductivity σ (in units e^2/h). (b) Electrical thermal conductivity κ_e (in units $k_B^2 T_0^2/h$). (c) Seebeck coefficient S (in units k_B/e). (d) figure of merit ZT of the c-2QD under attention in the $(\mu - \theta)$ plane. The left panels report the landscape of the thermoelectric functions in the $(\mu - \theta)$ plane, the right panels report sections of the same quantities at $\theta = 0, \pi/2, \pi, 3\pi/2$ and 2π. The black dashed lines in the right (c) and (d) panels evidence the results in the absence of magnetic flux. For $\theta = 2\pi$ no multiplication by 10 or by 100 has been performed, to better emphasize the enhancement effect of the magnetic field. The colored curves in the left panels respect the sequence of the graphs shown in the corresponding right panels.

figures 2(a) and (b) we observe that σ and κ_e have behavior similar to $\mathcal{T}$(E), as expected from their expressions; we also verified that the value of σ increases (not shown in the figures) decreasing the temperature, and that the opposite occurs for κ_e.

We observe that in the absence of magnetic field, i.e. $\theta = 0$, $\mathcal{T}$(E) presents a Breit-Wigner resonance around $E_b = -1$ eV, and similarly $\sigma(\mu, 0)$, and $\kappa_e(\mu, 0)$ present a Breit-Wigner resonance around $\mu = E_b$. Moreover, near the resonant energy the thermopower S vanishes while for $\mu \lesssim E_b$ ($\mu \gtrsim E_b$) S is negative (positive), indicating mainly n-type (p-type) behavior of the device. The figure of merit ZT vanishes where S vanishes as expected from its definition, and remains small (< 0.01) for any μ. As temperature increases both S and ZT values increase.

When the magnetic field is switched on, both Breit-Wigner- and Fano-like resonances may contribute to the transmission spectra. In particular, for $\theta = 2n\pi$, with n integer number, only Breit-Wigner resonances occur, which are located at the bonding energy for n even and at the antibonding energy for n odd [see equations (18)

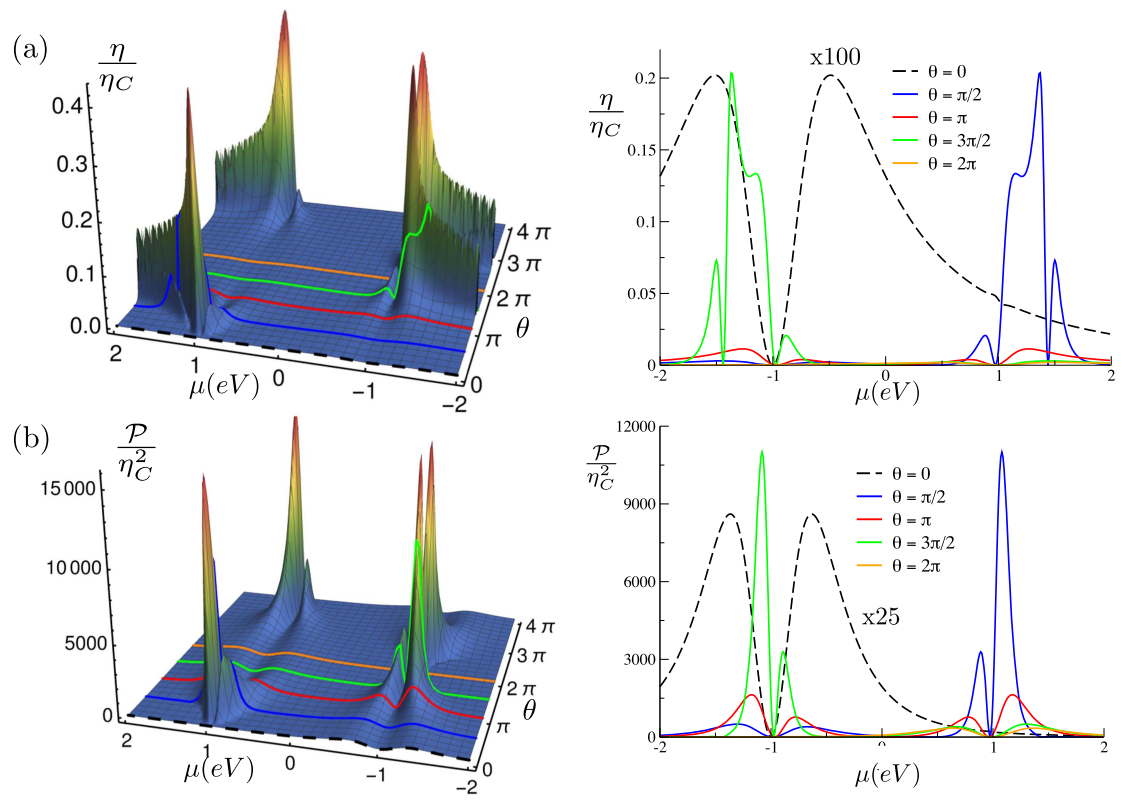

Figure 3. (a) Thermoelectric efficiency η/η_c in the $(\mu - \theta)$ plane. b) Output power $\mathcal{P}/\eta_c^2$ (in units $k_B^2 T_0^2/h$). The left panels of figures 3(a) and (b) report the landscape of the thermoelectric efficiency and power output in the $(\mu - \theta)$ plane, the right panels report sections of the same quantities at $\theta = 0, \pi/2, \pi, 3\pi/2$ and 2π. The black dashed lines in the right panels evidence the results in the absence of magnetic flux.

and (19)]. For $\theta = (\pi/2 + n\pi)$ both Breit-Wigner- and Fano-like resonances are present in the $\mathcal{T}$(E) spectrum, with Breit-Wigner (Fano) features centered at the bonding (antibonding) energies for n even and vice versa for n odd. We notice that $\mathcal{T}$(E) is symmetric around E_d for $\theta = \pi$ or $\theta = (2n + 1)\pi$ as required by equation (20). It is important to observe that $|S|$ increases by more than 10 times and ZT by more than 100 times with respect to the case $\theta = 0$, for specific values of the magnetic flux threading the c-2QD circuit as evidenced in the plots in the right side of figures 2(c) and (d). In particular $|S|$ assumes large values ($\approx 4k_B/e$) in the regions around $\theta \sim \pi/2$ and $\theta \sim 3\pi/2$ in the resonance and in the antiresonance regions. The above results are in agreement with the ones obtained for the benzene molecule junction in magnetic flux [40]. Figure 2(d) shows that for the chosen T and γ parameters, ZT can reach values $\approx$6 in the regions $\theta \sim \pi/2$ and $\theta \sim 3\pi/2$. The above results evidence that temperature and magnetic flux can be exploited to increase the thermoelectric factor of merit.

Most interesting is the evaluation of the performance of the c-2QD as heat engine, in this case a study of the efficiency at the maximum output power is required. Several recent papers [41–46] have shown that the mere knowledge of the maximum efficiency of a heat engine is of limited importance since the useful operative information concerns the conditions corresponding to the maximum power output [47, 48]. It is known in fact, that even if the figure of merit ZT of a thermoelectric device can assume large values ($\gg$1) mainly for nanostructured systems [10, 49, 50], what really matters is just the efficiency evaluated at the maximum power output.

To better clarify this point, we report in figure 3(a) the thermoelectric efficiency and in figure 3(b) the output power, respectively, as function of μ and θ, as defined in table 2.

Once again we observe that the magnetic field strongly enhances the thermoelectric efficiency by more than two orders of magnitude with respect to the case of absence of magnetic field, in the resonance and antiresonance regions, while output power increases more than 25 times and can assume values of the order of 10^4 (in units $k_B^2 T_0^2/h$). Figure 4 summarizes the results of the evaluation of the efficiency at the maximum power output, which is the most appropriate metric to measure the performance of the device. For this aim we have scanned the flux θ parameter in the [0–4π] range and, for any θ, we have looked for the maximum output power for varying values of the chemical potential μ. This has allowed to evaluate the efficiency for the values of θ and μ which determine the maximum power conditions.

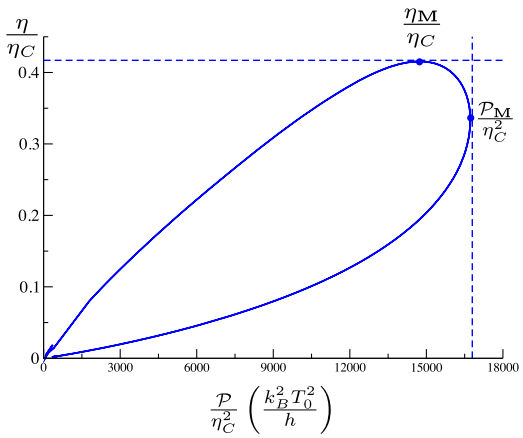

Figure 4. Maximum efficiency at the maximum output power. $\mathcal{P}_M/\eta_C^2$ is the highest value of the output power; η_M/η_C is the maximum value of the device efficiency.

The set of all the maximum power and corresponding efficiency data have been exploited to produce figure 4 which reports the curve of the maximum efficiency at the maximum output power. From figure 4 we can observe that the maximum efficiency is higher than the efficiency at operating conditions where the maximum output power is realized. We can see that the highest value of the power output $\mathcal{P}_M/\eta_C^2$ is 16800 (in units $k_B^2 T_0^2/h$) for the values $\theta \approx 1$, and $\theta \approx (4\pi - 1)$, at $\mu \approx 1.062$ eV, and for $\theta \approx (2\pi - 1)$ and $\theta \approx (2\pi + 1)$, at $\mu \approx -1.062$ eV. Correspondingly, the normalized efficiency at maximum power is $\eta(\mathcal{P}_M)/\eta_C = 0.33$. Moreover, we can see that the highest value of efficiency η_M/η_C is 0.43 which occurs for the values $\theta \approx \pi/4$ and $15\pi/4$, at $\mu \approx 1.068$ eV and for $\theta \approx 7\pi/4$ and $9\pi/4$, at $\mu \approx -1.068$ eV. Correspondingly, the power output is $\mathcal{P}(\eta_M)/\eta_C^2 = 14200$ (in units $k_B^2 T_0^2/h$).

Before concluding we verify explicitly that the results reported in figures 3 and 4 satisfy the general bounds for the output power worked out by Whitney [44, 51]. According to Whitney, the output power $\mathcal{P}$ for a single-channel heat engine, must satisfy the upper bound required by quantum mechanics

$$\mathcal{P} \leqslant A_0 \pi^2 \frac{k_B^2}{h} (T_L - T_R)^2 \equiv A_0 \pi^2 \frac{k_B^2 T_L^2}{h} \eta_c^2 \quad (with\ A_0 \pi^2 \approx 0.32)$$

where $\eta_c = (T_L - T_R)/T_L \quad (T_L > T_R)$ is the Carnot efficiency. The upper bound for the output power divided the the square of the Carnot efficiency becomes

$$\frac{\mathcal{P}}{\eta_c^2} \leqslant 0.32\, T_L^2 \frac{k_B^2}{h} = 0.32 \frac{T_L^2}{T_0^2} \frac{k_B^2 T_0^2}{h}$$

(where of course T_0 is chosen as the unit temperature in Kelvin degree). In the manuscript we have taken the temperature of the left reservoir $T_L = 300K$, and we arrive at the constraint

$$\frac{\mathcal{P}}{\eta_c^2} \leqslant 28000 \quad \left(in\ units\ \frac{k_B^2 T_0^2}{h}\right).$$

In figures 3 and 4 of our manuscript, the plotted values $\mathcal{P}/\eta_c^2$ extend in the range up to about 18000 (in units $k_B^2 T_0^2/h$), in agreement with the above constraint.

5. Conclusions

We have presented in this paper a systematic analytic study of the thermoelectric response functions of a coupled double quantum dot system, pierced by a magnetic field, connected to left and right reservoirs, in the linear regime. Our method is based on the Green's function formalism. The results are analytic and can be expressed in terms of easily accessible trigamma functions and Bernoulli numbers; this has allowed to scan wide ranges of values of chemical potentials and temperatures of the reservoirs, different threading magnetic fluxes, dot energies and interdot interactions. Our results show that thermoelectric transport through the c-2QD can be strongly enhanced by the magnetic flux, mainly in the energy regions around the bonding and antibonding resonances of the system, which can be experimentally reached varying the system chemical potential by appropriate gate. The thermopower S can be enhanced by more than ten times and the figure of merit ZT by more than hundred times by the presence of a threading magnetic field. Most important, we have also found in

this simple system that the magnetic flux increases the performance of the device under maximum power output conditions.

Acknowledgments

The authors acknowledge the 'IT center' of the University of Pisa for the computational support.

ORCID iDs

G Menichetti https://orcid.org/0000-0002-9588-5002

References

[1] Hicks L D and Dresselhaus M S 1993 *Phys. Rev.* B **47** 12727
[2] Sánchez D and Linke H 2014 *New J. Phys.* **16** 110201
[3] Pichard J-L and Whitney R S 2016 *Comptes Rendus Physique* **17** 1039
[4] Brogi B B, Chand S and Ahluwalia P K 2015 *Physica* B **461** 110
[5] Kang K and Cho S Y 2004 *J. Phys.: Condens. Matter* **16** 117
[6] Kubala B and König J 2002 *Phys. Rev.* B **65** 245301
[7] Blanter Y M, Bruder C, Fazio R and Schoeller H 1997 *Phys. Rev.* B **55** 4069
[8] Ladrón de Guevara M L, Claro F and Orellana P A 2003 *Phys. Rev.* B **67** 195335
[9] Gómez-Silva G, Ávalos-Ovando O, Ladrón de Guevara M L and Orellana P A 2012 *J. App. Phys.* **111** 053704
[10] Wierzbicki M and Swirkowicz R 2011 *Phys. Rev.* B **84** 075410
[11] García-Suárez V M, Ferradás R and Ferrer J 2013 *Phys. Rev.* B **88** 235417
[12] Wang Q, Xie H, Nie Y-H and Ren W 2013 *Phys. Rev.* B **87** 075102
[13] Orellana P A, Ladrón de Guevara M L and Claro F 2004 *Phys. Rev.* B **70** 233315
[14] Hofer P P and Sothmann B 2015 *Phys. Rev.* B **91** 195406
[15] Samuelsson P, Kheradsoud S and Sothmann B 2017 *Phys. Rev. Lett.* **118** 256801
[16] Bulka B R and Kostyrko T 2004 *Phys. Rev.* B **70** 205333
[17] Sierra M A, Saiz-Bretín M, Domínguez-Adame F and Sánchez D 2016 *Phys. Rev.* B **93** 235452
[18] Karwacki L and Trocha P 2016 *Phys. Rev.* B **94** 085418
[19] Bai Z-M, Yang M-F and Chen Y-C 2004 *J. Phys.: Condens. Matter* **16** 2053
[20] Liu Y S and Yang X F 2010 *J. App. Phys.* **108** 023710
[21] Pylak M and Svirkowicz T 2010 *Phys. Status Solidi* B **247** 122
[22] Sothmann B, Sánchez S and Jordan A N 2015 *Nanotechnology* **26** 032001
[23] Lambert C J, Sadeghi H and Al-Galiby Q H 2016 *Comptes Rendus Physique* **17** 1084
[24] Thierschmann H, Sánchez R, Sothmann B, Buhmann H and Molenkamp L W 2016 *Comptes Rendus Physique* **17** 1109
[25] Sánchez R R, Thierschmann H and Molenkamp L W 2017 *New J. Phys.* **19** 113040
[26] Erdman P A, Mazza F, Bosisio R, Benenti G, Fazio R and Taddei F 2017 *Phys. Rev.* B **95** 245432
[27] Svilans A, Leijnse M and Linke H 2016 *Comptes Rendus Physique* **17** 1096
[28] Nilsson M, Boström F V, Lehmann S, Dick K A, Leijnse M and Thelander C 2018 arXiv:1803.00326
[29] Nilsson M, Chen I-J, Lehmann S, Maulerova V, Dick K A and Thelander C 2017 *Nano Lett.* **17** 7847
[30] Dmitriev A V and Zvyagin I P 2010 *Physics Uspekhi* **53** 789
[31] Argüello-Luengo J, Sánchez D and López R 2015 *Phys. Rev.* B **91** 165431
[32] Gradshteyn I S and Ryzhik I M 1980 *tables of Integrals, Series and Products* (New York: Academic Press)
[33] Abramowitz M and Stegun I A 1972 *Handbook of Mathematical Functions* (New York: Dover)
[34] Butcher P 1990 *J. Phys. Cond. Matter* **2** 4869
[35] Grosso G and Pastori Parravicini G 2014 *Solid State Physics* 2nd edn (Oxford: Elsevier-Academic)
[36] Ferry D K, Goodnick S M and Bird J 2009 *Transport in Nanostructures* 2nd edn (New York: Cambridge University Press)
[37] Datta S 1997 *Electronic transport in Mesoscopic Systems* (Cambridge: Cambridge University Press)
Datta S 2005 *Quantum Transport: Atom to Transistor* (Cambridge: Cambridge University Press)
[38] Ashcroft N W and Mermin N D 1976 *Solid State Physics* (New York: Holt, Rinehart and Winston)
[39] Bevilacqua G, Grosso G, Menichetti G and Pastori Parravicini G 2016 *Phys. Rev.* B **94** 245419
[40] Li H, Wang Y, Kang X, Liu S and Li R 2017 *J. App. Phys.* **121** 065105
[41] Humphrey T E and Linke H 2005 *Phys. Rev. Lett.* **94** 096601
[42] Nakpathomkun N, Xu H Q and Linke H 2010 *Phys. Rev.* B **82** 235428
[43] Esposito M, Kawai R, Lindenberg K and Van den Broeck C 2010 *Phys. Rev. Lett.* **105** 150603
[44] Whitney R S 2014 *Phys. Rev. Lett.* **112** 130601
[45] Hershfield S, Muttalib K A and Nartowt B J 2013 *Phys. Rev.* B **88** 085426
[46] Luo X, Liu N and Qiu T 2016 *Phys. Rev.* E **93** 032125
[47] Curzon F L and Ahlborn B 1975 *Am. J. Phys.* **43** 22
[48] Benenti G, Casati G, Saito K and Whitney R S 2017 *Phys. Rep.* **694** 1
[49] Venkatasubramanian R, Siivola E, Colpitts T and O'Quinn B 2001 *Nature* **413** 597
[50] Murphy P, Mukerjee S and Moore J 2008 *Phys. Rev.* B **78** 161406(R)
[51] Whitney R S 2015 *Phys. Rev.* B **91** 115425